Research Article Vol. 7, No. 3 / March 2020 / Optica 209

Linear isolators using wavelength conversion

KAMAL ABDELSALAM,[1] TENGFEI LI,[2] JACOB B. KHURGIN,[2] AND SASAN FATHPOUR[1,3,*]

[1]CREOL, The College of Optics & Photonics, University of Central Florida, Orlando, Florida 32816, USA
[2]Department of Electrical and Computer Engineering, Johns Hopkins University, Baltimore, Maryland 21218, USA
[3]Department of Electrical and Computer Engineering, University of Central Florida, Orlando, Florida 32816, USA
*Corresponding author: fathpour@creol.ucf.edu

Received 12 December 2019; revised 27 January 2020; accepted 31 January 2020 (Doc. ID 385639); published 3 March 2020

Optical isolators, reliably integrated on-chip, are crucial components for a wide range of optical systems and applications. We introduce a new class of wideband nonmagnetic and linear optical isolators based on nonlinear frequency conversion and spectral filtering among the pump, signal, and idler wavelengths. The scheme is experimentally demonstrated using difference-frequency generation in periodically poled thin-film lithium niobate integrated devices and short- and long-pass optical filters. We demonstrate a wide bandwidth of more than 150 nm, limited only by the measurement setup, and an optical isolation ratio of up to 18 dB for the involved idler and signal waves. The difference of transmittance at the signal wavelength between forward and backward propagation is 40 dB. We also discuss pathways for substantial isolation improvement using appropriate anti-reflection coatings. The integrable isolator, operating in the telecommunication band, is characterized by a perfectly linear output versus input power dependence and can be incorporated into high-speed telecom and datacom systems as well as a variety of other applications.

https://doi.org/10.1364/OPTICA.385639

Optical isolators and circulators are essential components for signal routing and blocking in applications such as laser protection and stabilization and optical networks [1,2]. Their functionality is fundamentally based on breaking time-reversal symmetry or Lorentz reciprocity described by a symmetric scattering matrix [3–5]. Key features of an ideal optical isolator include broadband operation, linearity, low insertion loss, and high isolation. Another crucial feature for modern integrated photonic applications is small footprint required for integration of isolators with other components. Guided-wave isolators have been realized for decades using the Faraday effect in magneto-optical materials [6–8], where the garnet serves as the optical guiding layer. Introducing thin layers of garnets, e.g., yttrium iron garnet (YIG), to standard semiconductor-based photonic integrated circuits (PICs) has been pursued more recently with reasonable success [9–11]. Still, fabrication challenges, high insertion loss, and polarization dependence present formidable obstacles that prevent integrated magnetic isolators from being widely adapted. Hence, an alternative, nonmagnetic optical isolator has been vigorously pursued by many groups.

Lorentz reciprocity holds for any linear, time-invariant system with symmetric permittivity and permeability tensors. Thus, nonmagnetic optical nonreciprocity can be achieved through breaking either the linearity or time-invariance condition [3,5], often accompanied by introducing optical loss and gain. This has been sought by a number of research groups through adopting different approaches. For example, nonlinear effects [both second- $\chi^{(2)}$ and third-order $\chi^{(3)}$ nonlinearity] have been used [12–15]; however, these schemes have limited potential since their performance depends on input power or have limited operation bandwidth, and, furthermore, some of them are not even true isolators as explained in Ref. [4]. Recently, a theoretical modeling of a non-reciprocal system based on a parity-time symmetric scheme has been reported [16]. The proposed scheme incorporates ring resonators with alternating gain and loss in the presence of Kerr nonlinearity.

Meanwhile, true optical isolators based on time-varying modulation of material properties (usually refractive index) by a traveling wave of radio frequency (RF) have been proposed and investigated in recent years. These include electro-optically induced indirect inter-band transition [17,18], space-time modulation in photonic crystal waveguides [19], acousto-optic modulation [20,21] as well as electro-optic (EO) modulation in commercial devices [22,23], and more elaborate but conceptually similar work that involved synthetic angular momentum [24,25]. These schemes are truly isolating and linear, yet reliance on modulation at RF frequency leads to three deleterious effects. First, modulation at frequency of, say, 10 GHz limits the bandwidth of the signal to something less than that. Second, even if clever dispersion engineering can alleviate this problem, the presence of strong RF power inevitably causes high noise in the signal band—it may be not important if the isolator just serves to isolate the laser source, but it is problematic if it is used further along the optical path where the weak signal will be difficult to discern in the presence of a strong RF modulating wave. Last but not least, the working principle of all time-modulated schemes relies upon the fact that the processes that

are momentum (phase) matched in one direction are mismatched in the other direction. For instance, if the refractive index is modulated by a wave with a frequency Ω and wavevector $K(\Omega)$, the efficient energy transfer between two forward-propagating optical waves of frequencies ω_1 and $\omega_2 = \omega_1 - \Omega$ will be achieved when $k(\omega_1) = k(\omega_2) + K(\Omega)$ (i.e., when the group velocity of the optical wave matches the phase velocity of the RF wave). For backward propagation, the momentum mismatch is then $\Delta k = 2\,\mathrm{K}$, and the full isolation is attained if the length is chosen to be $L = \pi/K$. If the coupling wave is RF, the mismatch is relatively small (on the scale of reciprocal centimeters, cm^{-1}), and hence a long length is required. And any small deviation of length will cause leakage. To avoid this issue, one may consider acousto-optic modulation [20,21], where K is larger but then the bandwidth becomes severely limited.

All of these limitations, however, can be lifted once one realizes that in essence any time-dependent modulation scheme is a three-wave nonlinear parametric process. Hence, if instead of a low-frequency RF coupling wave one uses the wave of optical frequency, the bandwidth can be significantly expanded, no noise will enter the signal bandwidth, and, most important, the momentum mismatch K will become so large that no meaningful coupling in the backward direction can occur, leading to much higher and more robust isolation ratios.

This is precisely the idea behind this work, as we introduce a wholly new approach based on nonlinear frequency conversion processes [e.g., difference-frequency generation (DFG)] and spectral filtering to achieve nonmagnetic wideband and linear (in a sense of input versus output characteristics) optical isolation. The scheme is compatible with integrated photonics platforms, i.e., it can be potentially monolithically integrated on a single chip with complex PICs.

The operation principle of the new optical isolator is based on breaking Lorentz reciprocity in nonlinear waveguides. In essence, nonlinearity is one way to achieve an asymmetric scattering matrix ($S^T \neq S$) and hence non-reciprocal operation [3]. To explain the proposed concept, first consider the signal s and pump p co-propagation in the forward direction, shown in Fig. 1(a), with $\lambda_s < 2\lambda_p$. In this case, an idler wave can be generated at wavelength $\lambda_i = (\lambda_p^{-1} - \lambda_s^{-1})^{-1}$ through DFG, as long as the phase-matching condition is satisfied. The shown long-pass filter (LPF) at the output allows only the transmission of the idler, which now contains all the information transferred from the signal and blocks all other involved wavelengths. In Fig. 1(b), the signal and/or idler are coupled in the backward direction. The signal is blocked by the LPF, and only the idler can be transmitted. Since the pump and idler are counter-propagating in this case, the phase-matching condition is not satisfied, and hence, given that the wavevector mismatch is large (coherence length is on the scale of optical wavelength), no signal is generated, and the idler wave is eventually absorbed by the short-pass filter (SPF).

The frequency shift from signal to idler inherent in this scheme should not present a problem in most optical links, but if it does, it can be remedied by converting the idler output back to the input signal wavelength through another DFG process. Alternatively, as we have proposed elsewhere, the frequency shift can be completely avoided if sum-frequency generation (SFG) is used instead of DFG [26]. However, such a scheme would require a highly efficient SFG process in a long waveguide to achieve sufficient signal depletion and hence good isolation. It should be also noted that a

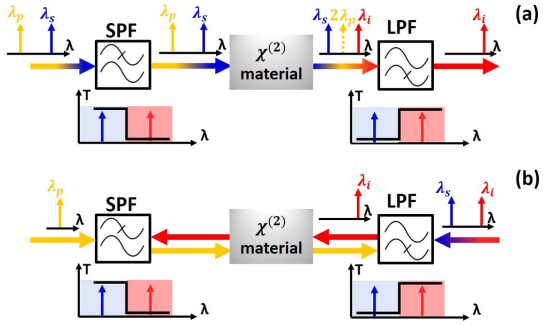

Fig. 1. Schematic diagram of the proposed optical isolator, showing operation principle in (a) forward and (b) backward directions. SPF, short-pass filter; LPF, long-pass filter.

combination of SFG and optical absorption can be used instead of filtering [27]. Again, long devices are needed to attain high conversion and efficient absorption. Also, the adiabatic rate of the quasi-phase-matching period is another restriction imposed in this scheme in order to avoid the overdamping problem due to strong absorption [27].

It should be mentioned that second-order nonlinearity in periodically poled lithium niobate (PPLN) has been exploited in the past to demonstrate optical isolation [12]. However, that scheme would only function at high input signal powers (1.5 W at 1550 nm), behaving more like a power limiter and lacking linearity. While our isolator is also based on second-order nonlinearity, its input–output relation is linear and not power dependent. In an ideal case, $P_i = \eta P_s P_p L^2$, where η is the nonlinear conversion efficiency and L is the length of PPLN, and thus the generated idler power is proportional to the input signal for a fixed pump power. Indeed, in our experiments the isolator works perfectly at low input pump powers of $\sim$3 mW.

In our proof-of-concept demonstration, we use a periodically poled thin-film lithium niobate (TFLN) waveguide as the $\chi^{(2)}$ nonlinear element and combine it with external spectral filters to achieve high isolation ratio. Details of the thin-film PPLN design and fabrication can be found in our previous work [28]. We have recently developed an actively monitored iterative poling technique to optimize the periodic poling conditions and have reported record-high efficiencies of up to 4600% $\mathrm{W}^{-1}\,\mathrm{cm}^{-2}$ [28]. The TFLN platform has many unique properties and is a fairly recent ultracompact platform on which a wide variety of integrated photonic components, such as highly efficient PPLN devices [28–31], high-speed optical modulators [32–34], cascaded nonlinear devices [35,36], quantum photonics devices [37,38] and acousto-optic devices [39,40] have been demonstrated.

An implementation of the proposed isolator system is depicted in Fig. 2. The thin-film PPLN waveguide is pumped using a dual pump (pump-signal) to generate a DFG signal at the telecommunication band. The pump source is a diode laser at 785 nm wavelength, which is tunable over few nanometers. The signal source is a continuous-wave (CW) laser that can be tuned from 1490 to 1640 nm. Inline polarization controllers (PCs) are used to adjust the pump and signal polarizations for transverse-electric (TE-)mode excitation into the waveguide. This guarantees utilizing the highest nonlinear coefficient of x-cut lithium niobate ($d_{33} = 30\,\mathrm{pm/V}$).

The signal is first filtered by a mechanically tunable SPF with a rolling-off slope of 20 dB/nm and a tuning range of 1490

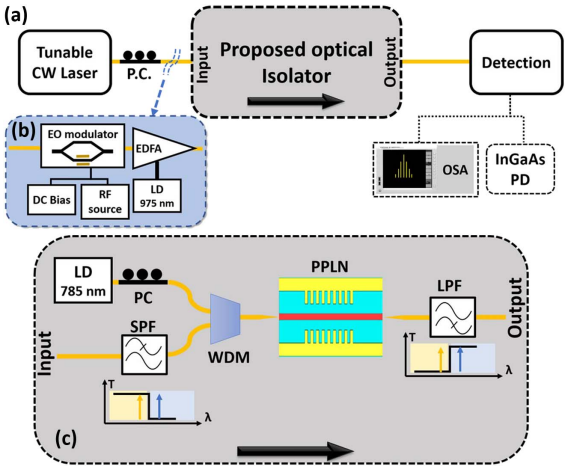

Fig. 2. Experimental setup for the demonstrated optical isolator with (a) the general scheme for forward measurement, (b) the added components for input modulation, and (c) the detailed schematic diagram of the optical isolator.

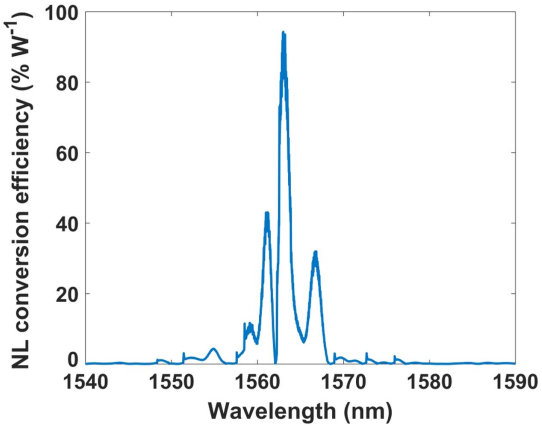

Fig. 3. Measured SHG efficiency versus pump wavelength shows a peak conversion efficiency of 95%W^{-1} around 1570 nm.

to 1610 nm. Then it is multiplexed with the pump through a wavelength-division multiplexer (WDM). The WDM output is coupled into the thin-film PPLN waveguide using an anti-reflection (AR)-coated lensed fiber. The output from the waveguide is also coupled using a similar lensed fiber and then filtered using a mechanically tunable LPF with similar specifications. The output is characterized using either an InGaAs detector at 1550 nm wavelength range or an optical spectrum analyzer (OSA).

Prior to the isolation experiments, we have characterized the PPLN waveguide by measuring the second-harmonic generation (SHG) and achieved nonlinear conversion efficiency of 95%W^{-1} in 4 mm long PPLN regions out of 1 cm long waveguides. This length can be significantly reduced without affecting the whole system's performance through using shorter PPLN devices with better poling uniformity and hence higher normalized efficiency. The measured phase-matching characteristics are shown in Fig. 3 with a phase-matching peak around $2\lambda_p = 1570$ nm. The observed deviation from an ideal sinc^2 function is attributed to statistical variation of fabrication parameters and poling nonuniformities over long lengths. This nonideality may be alleviated by adopting the techniques described in [41,42].

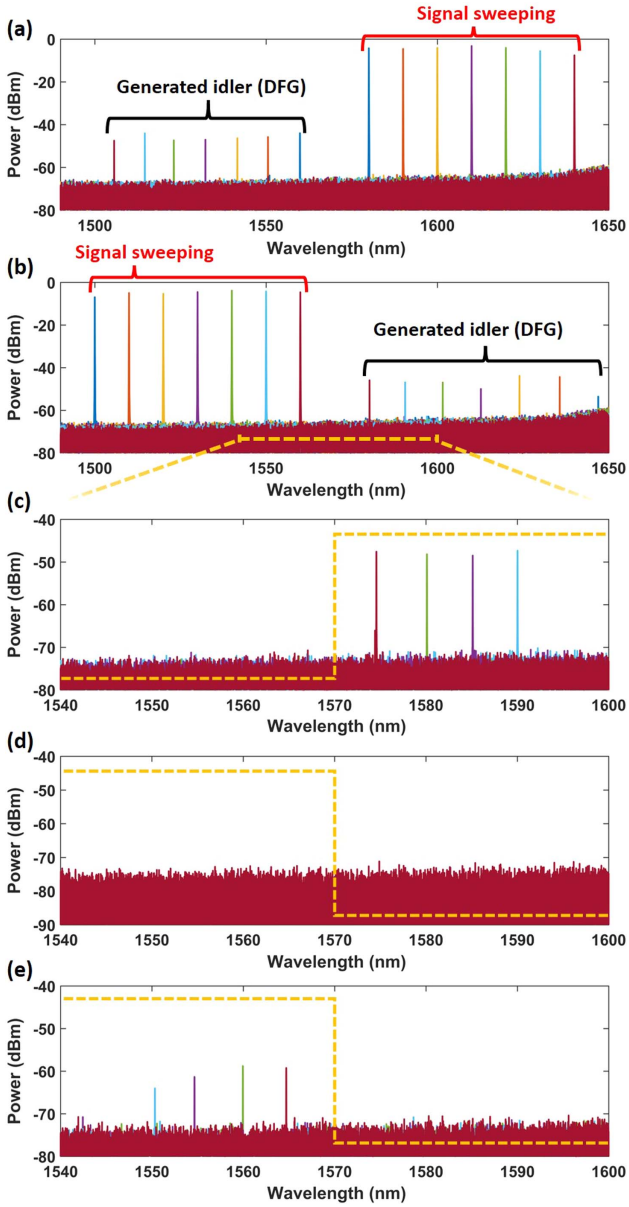

Fig. 4. Characterization results of the proposed isolator: Generated idler (DFG) measured before the LPF with signal tuned from (a) 1570 to 1640 nm and (b) 1500 to 1560 nm. Measured Isolator output in the (c) forward direction, (d) backward direction with tuned signal from 1550 to 1565 nm, and (e) backward direction with the idler coupled back and tuned from 1575 to 1590 nm. Dotted yellow lines represent the LPF and SPF transmission windows.

The experimental setup for characterizing the isolator is shown in Fig. 2(a). We first start with measuring the DFG signal. A wide tuning range of the DFG, extending from 1505 to 1646 nm, is attained as summarized in Figs. 4(a) and 4(b) and limited by the available tuning range of the CW signal laser. Then the output signal is measured after the LPF, demonstrating the forward-propagation case as shown in Fig. 4(c). Evidently, the signal and pump waves are completely blocked, and only the idler is transmitted with power level more than −50 dBm, carrying all the signal wave spectral information as desired. The signal wavelength is tuned from 1550 to 1565 nm, resulting in an idler wavelength tuned from 1575 to 1590 nm with a consistent power level. The overall insertion loss at the signal and idler wavelengths is ∼14 dB.

However, only ∼1 dB is attributed to the 1 cm TFLN device. The other 13 dB is due to coupling loss into the chip (∼3.7 dB per facet) and insertion losses of the WDM component (3 dB) and the two filters (1.3 dB, each), both of which can be reduced or eliminated in a fully integrated system.

Shown in Fig. 4(d) is the case where the backward-propagating signals below $2\lambda_p = 1570$ nm are completely blocked by the LPF, as far as the noise floor of the employed OSA (−75 dBm) suggests. This implies a difference of 40 dB between the forward- and backward-propagation transmittances at λ_s.

The isolation of the present isolator depends mainly on the filters' extinction ratios, nonlinear conversion efficiency, as well as any back-reflections of the involved pump, signal, and idler waves. Imagine a signal above 1570 nm is coupled in the isolator in backward direction. This can be the case if the forward-generated idler is back-reflected into the system. Such a signal is transmitted through the LPF. Although the phase-matching condition is not satisfied between this signal and the forward pump, as explained earlier, an output signal below 1570 nm with 13–18 dB less power than the forward case is evident in Fig. 4(e). In other words, the measured isolation is 13–18 dB, which is superior to most prior results obtained with time-varying schemes [18,19,21,23]. Isolations of 30 dB (at 2 GHz) and 14 dB (at 10 GHz) have been reported on an approach based on RF modulation [22]. However, as mentioned before, that approach suffers from inherently limited bandwidth and requires fine tuning.

The backward-propagating signal in the latter case is most likely generated through the DFG process between the backward-propagating idler and back-reflected pump from the PPLN devices' polished facet and any other reflections from other components and fibers. The backward-propagating pump power inside the PPLN is estimated to be 1 order of magnitude less than that of the forward-propagating pump based on the facet's reflectivity and insertion loss at the pump wavelength. This back-reflected pump and the backward-coupled signal waves hence co-propagate in the backward direction and satisfy the phase-matching condition, resulting in a relatively efficient DFG process. Then the generated signal could pass through the SPF at the output, tuned to block waves above 1570 nm, and get detected by the OSA and hence creating an isolation of 13–18 dB. This backward-generated signal can nonetheless be significantly reduced or eliminated by applying appropriately designed AR coatings to the PPLN facets and other system components to eliminate all back-reflections. The estimated isolation after AR coating is 40 dB, i.e., on par with the first case explained above.

For the sake of demonstrating applicability to optical communication systems, we examined the performance of our isolator when using RF-modulated optical signals. The RF modulation setup is shown in Fig. 2(b), in which an external RF commercial EO intensity modulator operating up to 13 GHz is employed. The modulating RF signal is generated by a network analyzer and amplified by an RF amplifier. The modulator is also DC biased for maximum sensitivity. The output from the modulator is amplified using an erbium-doped fiber amplifier (EDFA) to compensate for the insertion loss of the modulator. The laser signal, tuned from 1550 to 1565 nm, is first modulated with 5 GHz RF signal and coupled into the isolator.

Figure 5(a) shows the isolator output in the forward direction. The generated idler clearly carries all the information from the input signal represented by the modulation sidebands, shown in the zoomed output in the inset. The output power is a little bit lower than the unmodulated case due to the added sources of losses in the system but is still consistent over the tuning range. The input signal is then kept fixed at 1565 nm, the RF frequency is tuned from 5 to 11 GHz, and the output at 1575 nm is recorded for each frequency as reported in Fig. 5(b). This result demonstrates the isolator compatibility for high-speed communication, limited here only by the employed modulator bandwidth.

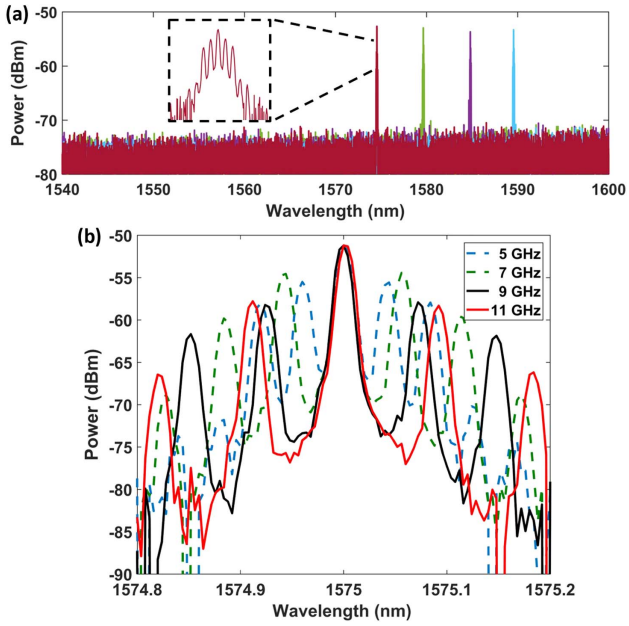

Fig. 5. Isolator output with RF modulated input signal at (a) fixed RF speed of 5 GHz and tuned optical signal (1550–1565 nm) and (b) tuned RF signal (5–11 GHz) and fixed input signal at 1565 nm.

Before concluding, we briefly outline the means by which the performance of the demonstrated isolator can be improved. The isolation ratio can be greatly improved by incorporating AR coatings and superior filters, the insertion loss can be reduced by improving coupling and eventually integrating all the components, and the conversion efficiency can be enhanced substantially if the pump, instead of being lost at the output LPF, can be rerouted back to the rear facet of the pump laser so the DFG can take place inside the ring pump laser cavity. It should be noted that this scheme is, in principle, a parametric amplifier. Hence, if the insertion loss is reduced significantly and efficiency is enhanced, the isolator can operate with gain rather than loss. It must be also mentioned that the proposed signal-to-idler isolation scheme is not limited to $\chi^{(2)}$ nonlinearity, as third-order nonlinear ($\chi^{(3)}$) processes, such as four-wave mixing (FWM), can be alternatively considered.

To summarize, we have proposed a novel class of nonmagnetic wideband linear optical isolators based on frequency conversion in nonlinear waveguides. We have demonstrated and characterized the performance of the proposed isolator using DFG in thin-film PPLN devices. The operational range of the isolator has extended from 1490 to 1640 nm, limited only by the bandwidth of the used equipment, and isolation up to 18 dB is measured for the idler and signal waves. The difference between forward- and backward-propagation transmittances at the signal wavelength is 40 dB. The isolator has demonstrated linearity and has shown no performance degradation with signals of up to 11 GHz in bandwidth, making it an attractive candidate for fully integrated photonics circuits.

Funding. Office of Naval Research (N000141712409); Division of Emerging Frontiers in Research and Innovation (1741694).

Disclosures. The authors declare no conflicts of interest.

REFERENCES

1. W. B. Ribbens, "An optical circulator," Appl. Opt. **4**, 1037–1038 (1965).
2. D. A. Miller, "Rationale and challenges for optical interconnects to electronic chips," Proc. IEEE **88**, 728–749 (2000).
3. D. Jalas, A. Petrov, M. Eich, W. Freude, S. Fan, Z. Yu, R. Baets, M. Popović, A. Melloni, and J. D. Joannopoulos, "What is—and what is not—an optical isolator," Nat. Photonics **7**, 579–582 (2013).
4. Y. Shi, Z. Yu, and S. Fan, "Limitations of nonlinear optical isolators due to dynamic reciprocity," Nat. Photonics **9**, 388–392 (2015).
5. D. L. Sounas and A. Alù, "Non-reciprocal photonics based on time modulation," Nat. Photonics **11**, 774–783 (2017).
6. Y. Okamura, H. Inuzuka, T. Kikuchi, and S. Yamamoto, "Nonreciprocal propagation in magnetooptic YIG rib waveguides," J. Lightwave Technol. **4**, 711–714 (1986).
7. T. Aichele, A. Lorenz, R. Hergt, and P. Görnert, "Garnet layers prepared by liquid phase epitaxy for microwave and magneto-optical applications–a review," Cryst. Res. Technol. **38**, 575–587 (2003).
8. H. Dötsch, N. Bahlmann, O. Zhuromskyy, M. Hammer, L. Wilkens, R. Gerhardt, P. Hertel, and A. F. Popkov, "Applications of magneto-optical waveguides in integrated optics," J. Opt. Soc. Am. B **22**, 240–253 (2005).
9. L. Bi, J. Hu, P. Jiang, D. H. Kim, G. F. Dionne, L. C. Kimerling, and C. Ross, "On-chip optical isolation in monolithically integrated non-reciprocal optical resonators," Nat. Photonics **5**, 758–762 (2011).
10. B. J. Stadler and T. Mizumoto, "Integrated magneto-optical materials and isolators: a review," IEEE Photon. J. **6**, 1–15 (2013).
11. P. Pintus, D. Huang, C. Zhang, Y. Shoji, T. Mizumoto, and J. E. Bowers, "Microring-based optical isolator and circulator with integrated electromagnet for silicon photonics," J. Lightwave Technol. **35**, 1429–1437 (2017).
12. K. Gallo, G. Assanto, K. R. Parameswaran, and M. M. Fejer, "All-optical diode in a periodically poled lithium niobate waveguide," Appl. Phys. Lett. **79**, 314–316 (2001).
13. L. Fan, J. Wang, L. T. Varghese, H. Shen, B. Niu, Y. Xuan, A. M. Weiner, and M. Qi, "An all-silicon passive optical diode," Science **335**, 447–450 (2012).
14. S. Hua, J. Wen, X. Jiang, Q. Hua, L. Jiang, and M. Xiao, "Demonstration of a chip-based optical isolator with parametric amplification," Nat. Commun. **7**, 13657 (2016).
15. P. Aleahmad, M. Khajavikhan, D. Christodoulides, and P. LiKamWa, "Integrated multi-port circulators for unidirectional optical information transport," Sci. Rep. **7**, 2129 (2017).
16. F. Nazari, N. Bender, H. Ramezani, M. Moravvej-Farshi, D. Christodoulides, and T. Kottos, "Optical isolation via PT-symmetric nonlinear Fano resonances," Opt. Express **22**, 9574–9584 (2014).
17. Z. Yu and S. Fan, "Complete optical isolation created by indirect interband photonic transitions," Nat. Photonics **3**, 91–94 (2009).
18. H. Lira, Z. Yu, S. Fan, and M. Lipson, "Electrically driven nonreciprocity induced by interband photonic transition on a silicon chip," Phys. Rev. Lett. **109**, 033901 (2012).
19. N. Chamanara, S. Taravati, Z.-L. Deck-Léger, and C. Caloz, "Optical isolation based on space-time engineered asymmetric photonic band gaps," Phys. Rev. B **96**, 155409 (2017).
20. Q. Wang, F. Xu, Z.-Y. Yu, X.-S. Qian, X.-K. Hu, Y.-Q. Lu, and H.-T. Wang, "A bidirectional tunable optical diode based on periodically poled $LiNbO_3$," Opt. Express **18**, 7340–7346 (2010).
21. J. Kim, S. Kim, and G. Bahl, "Complete linear optical isolation at the microscale with ultralow loss," Sci. Rep. **7**, 1647 (2017).
22. S. Bhandare, S. K. Ibrahim, D. Sandel, H. Zhang, F. Wust, and R. Noé, "Novel nonmagnetic 30-dB traveling-wave single-sideband optical isolator integrated in III/V material," IEEE J. Sel. Top. Quantum Electron. **11**, 417–421 (2005).
23. C. R. Doerr, N. Dupuis, and L. Zhang, "Optical isolator using two tandem phase modulators," Opt. Lett. **36**, 4293–4295 (2011).
24. D. L. Sounas and A. Alù, "Angular-momentum-biased nanorings to realize magnetic-free integrated optical isolation," ACS Photon. **1**, 198–204 (2014).
25. N. A. Estep, D. L. Sounas, J. Soric, and A. Alù, "Magnetic-free non-reciprocity and isolation based on parametrically modulated coupled-resonator loops," Nat. Phys. **10**, 923–927 (2014).
26. T. Li, K. Abdelsalam, S. Fathpour, and J. B. Khurgin, "Wide bandwidth, nonmagnetic linear optical isolators based on frequency conversion," in *CLEO: QELS_Fundamental Science* (Optical Society of America, 2019), paper FW3B. 7.
27. A. Rangelov and S. Longhi, "Nonlinear adiabatic optical isolator," Appl. Opt. **56**, 2991–2994 (2017).
28. A. Rao, K. Abdelsalam, T. Sjaardema, A. Honardoost, G. F. Camacho-Gonzalez, and S. Fathpour, "Actively-monitored periodic-poling in thin-film lithium niobate photonic waveguides with ultrahigh nonlinear conversion efficiency of 4600% W^{-1} cm^{-2}," Opt. Express **27**, 25920–25930 (2019).
29. L. Chang, Y. Li, N. Volet, L. Wang, J. Peters, and J. E. Bowers, "Thin film wavelength converters for photonic integrated circuits," Optica **3**, 531–535 (2016).
30. C. Wang, C. Langrock, A. Marandi, M. Jankowski, M. Zhang, B. Desiatov, M. M. Fejer, and M. Lončar, "Ultrahigh-efficiency wavelength conversion in nanophotonic periodically poled lithium niobate waveguides," Optica **5**, 1438–1441 (2018).
31. S. Fathpour, "Heterogeneous nonlinear integrated photonics," IEEE J. Quantum Electron. **54**, 1–16 (2018).
32. A. Rao, A. Patil, P. Rabiei, A. Honardoost, R. DeSalvo, A. Paolella, and S. Fathpour, "High-performance and linear thin-film lithium niobate Mach–Zehnder modulators on silicon up to 50 GHz," Opt. Lett. **41**, 5700–5703 (2016).
33. P. O. Weigel, J. Zhao, K. Fang, H. Al-Rubaye, D. Trotter, D. Hood, J. Mudrick, C. Dallo, A. T. Pomerene, and A. L. Starbuck, "Bonded thin film lithium niobate modulator on a silicon photonics platform exceeding 100 GHz 3-dB electrical modulation bandwidth," Opt. Express **26**, 23728–23739 (2018).
34. C. Wang, M. Zhang, X. Chen, M. Bertrand, A. Shams-Ansari, S. Chandrasekhar, P. Winzer, and M. Lončar, "Integrated lithium niobate electro-optic modulators operating at CMOS-compatible voltages," Nature **562**, 101–104 (2018).
35. A. Honardoost, G. F. C. Gonzalez, S. Khan, M. Malinowski, A. Rao, J.-E. Tremblay, A. Yadav, K. Richardson, M. C. Wu, and S. Fathpour, "Cascaded integration of optical waveguides with third-order nonlinearity with lithium niobate waveguides on silicon substrates," IEEE Photon. J. **10**, 1–9 (2018).
36. T. Sjaardema, A. Rao, and S. Fathpour, "Third-and fourth-harmonic generation in cascaded periodically-poled lithium niobate ultracompact waveguides on silicon," in *CLEO: Science and Innovations* (Optical Society of America, 2019), paper STh1J. 1.
37. J. Zhao, C. Ma, M. Rüsing, and S. Mookherjea, "Entangled photon-pair generation in periodically-poled thin-film lithium niobate waveguides," arXiv:1910.03202 (2019).
38. B. S. Elkus, K. Abdelsalam, A. Rao, V. Velev, S. Fathpour, P. Kumar, and G. S. Kanter, "Generation of broadband correlated photon-pairs in short thin-film lithium-niobate waveguides," Opt. Express **27**, 38521–38531 (2019).
39. L. Cai, A. Mahmoud, M. Khan, M. Mahmoud, T. Mukherjee, J. Bain, and G. Piazza, "Acousto-optical modulation of thin film lithium niobate waveguide devices," Photon. Res. **7**, 1003–1013 (2019).
40. L. Cai, A. Mahmoud, and G. Piazza, "Low-loss waveguides on Y-cut thin film lithium niobate: towards acousto-optic applications," Opt. Express **27**, 9794–9802 (2019).
41. J. T. Nagy and R. M. Reano, "Periodic poling of ion-sliced X-cut magnesium oxide doped lithium niobate thin films," in *Conference on Lasers and Electro-Optics* (Optical Society of America, 2018), paper JTh3C. 2.
42. J. Zhao, M. Rüsing, and S. Mookherjea, "Optical diagnostic methods for monitoring the poling of thin-film lithium niobate waveguides," Opt. Express **27**, 12025–12038 (2019).